AIP | Physics of Fluids

Using sharp transitions in contact angle hysteresis to move, deflect, and sort droplets on a superhydrophobic surface

Michael A. Nilsson and Jonathan P. Rothstein

Citation: Phys. Fluids **24**, 062001 (2012); doi: 10.1063/1.4723866
View online: http://dx.doi.org/10.1063/1.4723866
View Table of Contents: http://pof.aip.org/resource/1/PHFLE6/v24/i6
Published by the American Institute of Physics.

Using sharp transitions in contact angle hysteresis to move, deflect, and sort droplets on a superhydrophobic surface

Michael A. Nilsson and Jonathan P. Rothstein[a)]
Department of Mechanical and Industrial Engineering, University of Massachusetts – Amherst, Amherst, Massachusetts 01003-2210, USA

(Received 27 September 2011; accepted 16 May 2012; published online 8 June 2012)

In order to make an effective droplet-based microfluidic device, one must be able to precisely control a number of key processes including droplet positioning, motion, coalescence, mixing, and sorting. In a typical three-dimensional device, these processes are well understood. However, for planar or open microfluidic devices, many of these processes have yet to be demonstrated. In this paper, a series of superhydrophobic surfaces created by sanding Teflon are used as the microfluidics platform. The superhydrophobic surfaces used in this study all have advancing contact angles of 150° but have contact angle hysteresis that were varied smoothly from 3° to 30° as the grit size of the sandpaper is changed. Drop motion was initiated by placing the surface on an inclined plane. To deflect and move droplets along the surface, single and multiple transition lines in receding contact angle were created by spatially varying the surface roughness of the Teflon. The degree of droplet deflection was studied as a function of droplet size, droplet speed, and the angle that the transition line in contact angle hysteresis made with the principle direction of droplet motion. Droplet deflections across a single transition as large as 140% the droplet diameter were observed. The droplet deflection was found to increase with increasing difference in contact angle hysteresis across the transition and increasing transition angles up to about 40°. The largest deflections were observed over a very narrow range of droplet velocities corresponding to a range in Weber numbers between 0.1 and 0.2. This narrow range in Weber number suggests that transitions in receding contact angle can be used to sort drops based on velocity, size or wetting properties with a strong degree of selectivity. The direction of deflection was observed to change depending on whether the drops transitioned from a region of low to high or high to low contact angle hysteresis. In a transition from low to high hysteresis, a large portion of the drop's kinetic energy is converted into interfacial energy as the receding contact line of the drop is deformed. Alternatively, a transition from high to low hysteresis results in some of the drop's interfacial energy converted into kinetic energy as the deformation of the droplet is reduced. The result is either a reduction or increase in the droplet's velocity normal to the line of transition depending on the sign of the transition in contact angle hysteresis. Finally, single and multiple stripes of different contact angle hysteresis are also shown to be effective at deflecting droplets.
 [http://dx.doi.org/10.1063/1.4723866]

I. INTRODUCTION

Microfluidics has become an important and widely studied and implemented platform for diagnostics, material characterization, synthesis, and formulation over the past few decades.[1–6]

[a)]Author to whom correspondence should be addressed. Electronic mail: rothstein@ecs.umass.edu.

The main advantage of microfluidics is that small volumes of fluid can be precisely controlled and manipulated. Microfluidic devices are typically enclosed devices, created in a polymer such as polydimethylsiloxane or glass via photolithography. These are often single application or one-time-use devices due to the tendency for micro-scale channels to clog or degrade after sustained use. Additionally, in microfluidic devices, it is often advantageous to perform experiments using individual drops of fluid rather than streams. This is a field often referred to as digital microfluidics because the drop is manipulated one drop at a time rather than as a continuous flow. The major advantage of using droplets is that it allows one to manipulate individual plugs of fluid while avoiding dispersion effects.

In this field of digital microfluidics, there are a number of key challenges that must be addressed if the device is to be successful. These include droplet positioning, movement, coalescence and mixing, splitting, and finally droplet deflection. In this work, we will demonstrate a new method for addressing two of these challenges: droplet positioning and deflection. What makes our devices unique are that the droplets are manipulated and deflected on an open two-dimensional substrate without the use of an enclosed channel as is done in conventional microfluidic devices. Our microfluidic devices consist of planar superhydrophobic surfaces with discrete spatial variations in wetting properties, specifically contact angle hysteresis. Superhydrophobic surfaces can be fabricated in a number of ways.[7] Here, the devices are fabricated by mechanically sanding Teflon with sandpaper of various grit-designations to produce a randomly rough surface.[8] The superhydrophobic surfaces are inexpensive and easy to fabricate. In addition, by varying the sandpaper roughness, surfaces with a wide range of both advancing contact angles and contact angle hysteresis can be fabricated, allowing for the systematic and independent variation of either property.

Contact angle hysteresis is defined as the difference in advancing and receding contact angles, $\theta_H = \theta_A - \theta_R$. Contact angle hysteresis inhibits contact line motion through a sticking force that goes as[9]

$$F_D \approx \gamma l(\cos(\theta_R) - \cos(\theta_A)). \tag{1}$$

Here, γ is the surface tension and $l = R\sin(\pi - \theta)$ is the radius of the contact area between the drop and the surface. In order for a droplet to move, the droplet must first deform such that the advancing contact angle is exceeded and the receding contact angle is surpassed. In this work, all of the Teflon surfaces have an advancing contact angle of $\theta_A = 150^\circ$ but vary in receding contact angle resulting in contact angle hysteresis that range from 3° to 50°. In Nilsson and Rothstein,[10] these surfaces were utilized to investigate the effect of contact angle hysteresis on droplet coalescence and mixing. They showed that reduction in contact angle hysteresis can dramatically improve droplet mobility, deformation, and mixing following droplet coalescence.

Over the last few years there has been quite a bit of work in the field of two-dimensional digital microfluidics with a focus primarily on droplet motion. Superhydrophobic surfaces are the primary platform for drop studies as they are inspired by the remarkable behavior of water droplets on the leaves of the lotus plant.[11] Droplets on surfaces with little contact angle hysteresis have been found to be extremely mobile and as such are very sensitive to vibrations and small perturbations.[12–16] Droplet motion across superhydrophobic surfaces has also generated much interest. By tracking a single particle near the surface of a drop, Richard and Quere[17] have shown that viscous droplets with high contact angles on a surface tend to roll across the surface in agreement with theory.[18] The solid-body motion of the rolling drop greatly reduces the resistance to motion and has been shown to reduce the drag on the drops by as much as 99%.[14] Gogte *et al.*[19] later showed that for water on superhydrophobic textured surface, droplets initially slide at times near the onset of motion. They found that as the droplet accelerates it transitions to rolling motion. During the early stages of drop motion, the droplets trajectory approaches the free fall limit and interestingly it accelerates faster than a solid sphere rolling down the same inclined surface.[20]

In each of the experiments described above, droplet motion was induced by placing the substrate on an incline. Droplet motion can be induced in a number of other ways. Droplets can be moved based off of wettability gradients in patterned superhydrophobic surfaces.[21–23] For example, Wier *et al.*[24] have shown that they can produce spontaneous droplet motion by spatially varying the surface chemistry and the advancing contact angles across a surface with minimal contact angle hysteresis.

A number of active methods exist for manipulating drops. These include mechanical actuation of the surface, aerodynamically driving drop motion through a puff of air,[10] or building electrodes into the surface to induce motion of the droplets through electrowetting.[25] Krupenkin *et al.*[26] demonstrated the ability to change wettability characteristics by using an electrode inserted in a droplet and a dc electrical field to drive a droplet from a superhydrophobic state to completely wetting. Optical-electric devices can be used to direct a motion of a drop as it falls by optically sensing the position of drops and then activating a charging device to alter drop trajectory.[27] Electro-wetting devices can also be used to perform coalescence, mixing, and sorting of droplets.[28] However, these devices tend to be expensive and complicated to fabricate. In this work, our goal is to develop an inexpensive passive technique to manipulate drop motion.

A number of previous studies have investigated the motion of droplets traversing over discrete changes in surface wettability. Suzuki *et al.*[29] have shown that a droplet's trajectory can be passively altered by using different surface chemistries to create an array of wetting and non-wetting stripes aligned at an oblique angle to the primary direction of droplet motion. Both the wetting and non-wetting stripes had similar degrees of contact angle hysteresis, $\theta_H = 16^\circ$ but very different advancing and receding contact angles. In their work, a series of arrays of 500 μm and 100 μm stripes were placed on an incline at an angle of 35° from horizontal and oriented at various in plane angles. The velocity of the droplets was found to oscillate as they progressed across the striped surface. For the smallest droplets tested, a maximum droplet deflection angle of 13° was observed.[29] The droplets were always found to deflect towards the directions of the stripes to minimize drag, in a manner similar to continuous flows past striped and grooved surfaces.[30–32] A number of open questions still remain, the most interesting being what happens when a droplet flows past a single wettability transition rather than an array of stripes because it addresses the underlying physics of droplet deflection. Weir *et al.*[24] hypothesized that a two-dimensional digital microfluidic device could be designed to utilize a drop's reluctance to cross from a region of lower to higher advancing contact angle to affect droplet trajectory. They showed that the additional gravitational potential energy needed to advance from a region of low to high contact angle can often be enough to exclude a slowly moving droplet from advancing onto the high contact angle surface. In this way, they were able to demonstrate the ability to steer droplets along a surface by drawing boundaries of high contact angle on a low contact angle background. The devices developed in this paper will implement and test some of the conjecture of Weir *et al.*[24] by creating surfaces with constant advancing contact angles but with sharp transitions in receding contact angle and studying their ability to deflect, sort, and capture drops.

II. SUPERHYDROPHOBIC SURFACE FABRICATION

When a superhydrophobic surface has a precisely patterned or randomly patterned surface roughness capable of supporting an air-water interface, it is said to be in a Cassie-Baxter state of wetting.[33] The Cassie-Baxter state typically has both high advancing contact angles ($\theta_A \geq 150^\circ$) and minimal hysteresis. As a result, droplets tend to have high mobility. When the roughness is not ideal and is too wide, shallow, or rounded to support an air-water interface the water permeates and fully wets roughened surface, resulting in a droplet in the Wenzel state.[34] The Wenzel state may have high advancing contact angles but also characteristically has a high contact angle hysteresis. The work presented here will employ surfaces in both the Cassie and Wenzel states and utilize discrete transitions in droplet wetting from one state to the other to deflect droplets based on size, speed, and composition.

The basic surface preparation technique used in this experiment is detailed in Nilsson *et al.*[8] In their work, they showed that sanding Teflon with different grits of sandpaper can produce randomly patterned surfaces with different degrees of roughness. With this technique a wide range of advancing and receding contact angles could be achieved simply by choosing the appropriate sandpapers. In this study, we will focus on a series of sanded Teflon surfaces for which the advancing contact angle can be held fixed at $\theta_A = 150^\circ$ but which have a receding contact angle that varies from 120° to 147°. To generate the superhydrophobic surfaces used in this study, small pieces of Teflon were initially mounted to an aluminum substrate with epoxy to ensure a flat level surface. To create the wetting

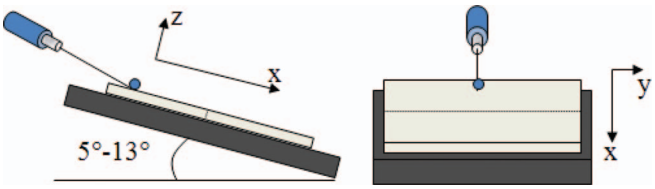

FIG. 1. Schematic diagram of the experimental setup. The transition from one contact angle hysteresis to another is shown as a dashed line.

transitions, the entire Teflon surface was initially sanded with a sandpaper of one grit designation. Non-marking model tape was placed over half of the surface and the exposed half was then re-sanded with a sandpaper of a different grit designation. Care was taken to not tear or rip the tape during the second sanding. The tape was removed, and the surface cleaned with acetone, deionized water, and blown dry with pressurized air. The resulting Teflon surface contains two distinct regions of similar advancing contact angle ($\theta_A = 150^\circ$) but varying receding contact angles, with a sharp transition between them as shown in Figure 1.

III. RESULTS AND DISCUSSION

The patterned Teflon surfaces were then placed on a plane with an adjustable inclination angle, α, to induce droplet motion. The inclination angle required to initiate the motion of the water droplet is dependent on both the contact angle hysteresis and the droplet size. Only for droplets where the gravitation force exceeds the sticking force, $mg \sin\alpha > F_D$, will the droplets move down the incline. Expanding both sides for nearly spherical droplets, we find a critical inclination of $\sin\alpha_{\text{crit}} = \frac{(\kappa^{-1})^2 \sin(\pi-\theta)(\cos\theta_R - \cos\theta_A)}{4/3\pi\ R^2}$. As a result, there are cases for very small droplets or large contact angle hysteresis surfaces where droplets will remain pinned even on vertically oriented surfaces. Here, $\kappa^{-1} = \sqrt{\gamma/\rho g}$ is the capillary length which for water is $\kappa^{-1} = 2.7$ mm and $\theta = (\theta_A + \theta_R)/2$ is the average contact angle used in the calculation of the length of the contact line. Once moving, Reyssat *et al.*[20] showed that on a superhydrophobic surface the total force acting on the droplet becomes the gravitational force minus the sticking force introduced by contact angle hysteresis, $F_{tot} = mg \sin\alpha - F_D$. Substituting in for sticking force from Eq. (1) and expanding for nearly spherical drops, one finds

$$\frac{F_{tot}}{mg\ \sin\alpha} = \left(1 - \frac{(\kappa^{-1})^2 \sin(\pi - \theta)(\cos\theta_R - \cos\theta_A)}{4/3\pi\ R^2 \sin\alpha}\right). \tag{2}$$

Reyssat *et al.*[20] showed that for surfaces with very low contact angle hysteresis the effect of the sticking force is minimal, accounting for only a few percent change in the total force acting on the droplet. In their study, droplets were observed to descend down the superhydrophobic surface following the law of free fall until a terminal velocity was reached as aerodynamic and viscous forces slowed and deformed the sliding droplet. Here, we investigate the effect of hysteresis on the drag of a drop keeping the advancing contact angle fixed at $\theta_A = 150^\circ$. In Figure 2, the total force on the droplets is presented normalized by the force of gravity for droplets. Using a micropipette, droplets of de-ionized water were placed on a sanded Teflon surfaces inclined at 13° above horizontal. All of the droplets were initially placed on and allowed to accelerate down a low hysteresis surface, $\theta_H = 3^\circ$, before transitioning to a surface with higher hysteresis. The droplets moved easily down the low hysteresis surface under gravity and accelerated towards the contact angle transition reaching it at a velocity of approximately $U \approx 0.12$ m/s. By bringing droplets onto the higher hysteresis surfaces with a non-zero velocity, it was possible to observe droplet motion and calculate drag forces on surfaces where the droplets were observed to decelerate at the inclination angle chosen.

A high-speed camera (Phantom v4.2) was used to capture the droplet motion at a frame rate of 2900 fps. The acceleration of the drops was measured from the high-speed video images at a position $x = 2$ mm downstream of the contact angle transition and used to calculate the total force on the drop to compare with the theoretical predictions of Eq. (2). As expected, the total driving force

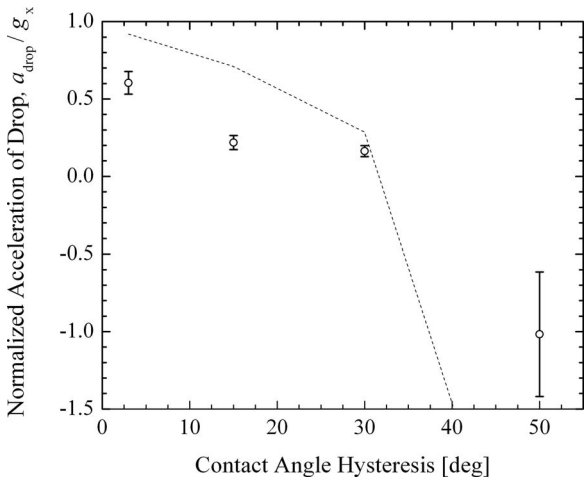

FIG. 2. The normalized acceleration of a 3.5 mm diameter droplet moving down an inclined plane of variable contact angle hysteresis and constant advancing contact angle of $\theta_A = 150^\circ$ as compared to the theory developed in Eq. (2) (dashed line).

is found to decrease with increasing contact angle hysteresis as the sticking force increases. As seen in Figure 2, the sticking force on the droplets with $\theta_H \leq 30^\circ$ is less than the force of gravity and as a result the drops are observed to accelerate down the length of the inclined superhydrophobic surface. The hysteretic drag on droplets on the smooth Teflon (50° hysteresis), however, is much larger than gravity and the drops are quickly decelerated. In the Cassie-Baxter state, the presence of the air-water interface can induce slip and dramatically reduce drag.[9,20] In fact, for very low hysteresis surfaces the viscous drag can be completely ignored.[14,17,20] Contrast this to the higher hysteresis surfaces in which the water is in contact with less trapped air and to some degree has reverted to the fully wetted Wenzel state in which the droplet must flow over a rough no-slip surface. In both cases, increased hysteresis corresponds not only to an increased sticking force but also a small viscous drag component. Although the experiments and theory agree qualitatively, the experimentally observed drag on the droplets is underpredicted by Eq. (2) at low hysteresis and overpredicted at high values of hysteresis. This is likely due to the fact that Eq. (2) ignores effects of viscous losses and assumes nearly spherical drop shape.

The difference in drag along a surface of different hysteresis suggests that if the transition were not perpendicular to the flow direction, but at some oblique angle, the droplets could be deflected. Additionally, the large deceleration and drag measured on the smooth Teflon suggests that it could be used to capture and collect a drop moving along a surface of lower hysteresis. To investigate these hypotheses, the sanded Teflon surfaces were mounted on a rotating stage to change the in plane angle of the transition, α_T, while varying the incline between 10° and 13° to achieve the desired variation in droplet velocity and Weber number. This experimental setup can be seen schematically in Figure 3. The deflection distance, d, is the distance a drop moves from the original trajectory after passing the sharp transition in receding contact angle. This deflection distance is measured at a location 15 mm downstream of the transition because by the time the droplet passes this distance any lateral motion has ceased and the droplet motion again is straight downhill. The deflection distance is normalized by the droplet diameter in the figures that follow. The droplet diameters in this study were 3.6 mm on average with a standard deviation of 0.1. Positive deflections indicate deflection to the left while negative deflections are to the right. The deflection is a function of Weber number, $We = \rho U^2 D/\gamma$, which is a dimensionless group that indicates the relative importance of inertial forces to interfacial forces Here, U is the velocity as it arrives at the transition, ρ is the density of the fluid, D is the diameter of the droplet, and γ is the surface tension of the fluid. At large Weber numbers, inertial forces dominate while at low Weber numbers capillary forces dominate. On a given surface in this work, the Weber number could be varied below 1.25 and the angle of the transition line, α_T, was varied incrementally from 0° to 45°. A wide variety of hysteresis transitions were fabricated. The high-speed camera was mounted atop a tripod with the camera tilted to allow

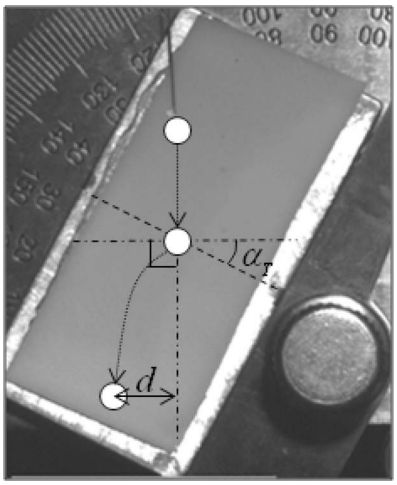

FIG. 3. Experimental setup with important parameters overlaid. The dashed line represents the location of the transition in contact angle hysteresis transition.

for a view perpendicular to the surface. For consistency, the data presented here are for surfaces rotated clockwise. However, the behavior was symmetric and the resulting dynamics were found to be independent of rotation direction.

Regardless of the particular contact hysteresis involved, when a droplet moves from a surface of high contact angle hysteresis to one with low contact angle hysteresis, the resulting deflection is always towards the left. This can be seen in the left hand figures in Figure 4 both as an overlay of several images of a drop as it progresses along the surface and as a schematic diagram that we will use to better explain the physics. Conversely, when a droplet moves from a surface with low contact angle hysteresis to one with high contact angle hysteresis the droplet deflected is always towards the right. This is illustrated in the images and the schematic diagrams in the right hand side of Figure 4. The directionality of the deflections is caused by the dynamics of the receding contact line as it encounters the transition. Recall that in all cases the advancing contact angle is identical and only the receding contact angle is affected by the transition. In the case a transition from high to low contact angle hysteresis upstream of the transition, the droplet is initially moving with a lower receding contact angle. The droplet deformation required to move along the high hysteresis surface upstream of the transition results in significant interfacial energy being stored within the moving, deformed droplet. Upon reaching and passing the transition, the receding contact angle is reduced and the backside of the drop quickly retracts. The droplet becomes less deformed and approaches

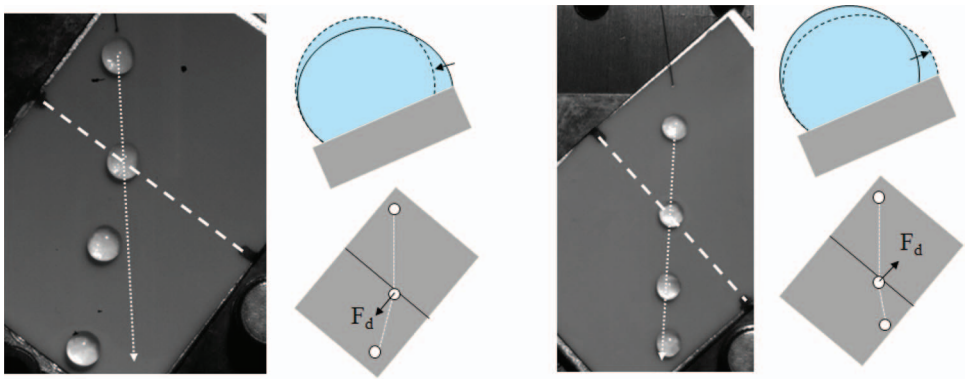

FIG. 4. Sample droplet trajectories for transitions (on the left) from higher to lower contact angle hysteresis and (on the right) from lower to higher contact angle hysteresis.

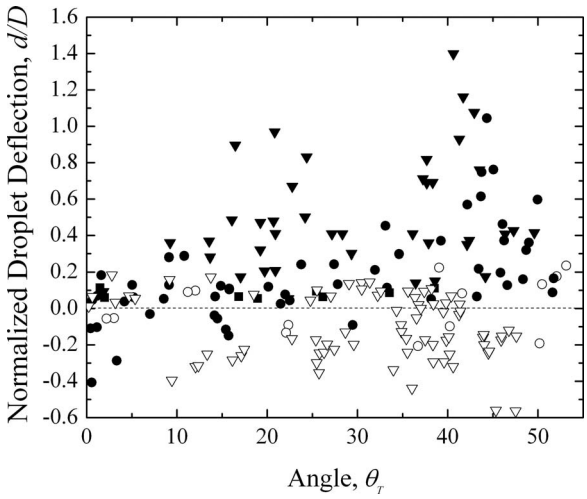

FIG. 5. Deflection of drops moving over a single transition in contact angle hysteresis presented as a function of the angle of transition, α_T, for a range of Weber numbers between 0.05 and 1.25. The data include transitions from (■) 3° to 50°, (○) 3° to 15°, (●)15° to 3°, (▽) 3° to 30°, and (▼) 30° to 3°.

a spherical shape. The sudden release of stored potential energy provides a small force that acts to accelerate the droplet normal to the contact angle hysteresis transition. This is shown schematically in Figure 4. The small driving force is equivalent to the difference in the sticking force in Eq. (1) between the high and low hysteresis surfaces,

$$F_{\text{Deflection}} \approx \gamma R \sin(\pi - \theta)(\cos(\theta_R)_1 - \cos(\theta_R)_2). \tag{3}$$

Here, $(\theta_R)_1$ corresponds to the receding contact angle of the upstream surface and $(\theta_R)_2$ to the downstream surface. This force is aligned perpendicular to the transition angle. Conversely, for a transition from low to high contact angle hysteresis, the droplet is deformed from a nearly spherical shape to a more deformed shape. In this process, some kinetic energy is removed from the drop and converted to an increase in interfacial energy. The result is a force that decelerates the drop in a direction normal to the transition line. As seen in Figure 4, the result is a deflection of the drop to the right. Note that this observation is different from that of Suzuki *et al.*[29] for flow of a droplet across a surface with stripes of variable wettability. In their experiments, droplet deflection was always found to occur towards the orientation of the stripes. In the context of our experiments, the droplet deflections observed by Suzuki *et al.*[29] would be to the right.

The magnitude of the resulting deflection for a given transition angle and transition in contact angle hysteresis is shown in Figure 5 for a wide range of Weber numbers between 0.05 and 1.25. One clear observation is that the deflection of droplets is much larger when the droplet transitions from a surface with higher contact angle hysteresis to one with lower contact angle hysteresis. This is true even if the Weber number, transition angle, and the magnitude of the change in hysteresis are identical. The response of a droplet to a transition in receding contact angle is not reversible. This observation is not intuitive, as in this case the amount of energy added or removed by the receding contact line dynamics is the same as is the magnitude of the deflection force calculated from Eq. (3). If one investigates the angle that the droplet trajectory is altered when transitioning from 30° to 3° and 3° to 30° hysteresis, the angles are identical in magnitude for any given Weber number experiment. This observation indicates that transition has induced the same amount of transverse velocity in each case. Take, for example, a Weber number of 0.15 and transition angle of $\alpha_T = 40°$. In this case, both drop trajectories are altered by 14° to the left for the 30° to 3° transition and 14° to the right for the 3° to 30° hysteresis transition. In previous work with micrometer-sized stripes of varying wettability, similar deflection angles were also observed.[29] Because the deflection angle is identical in both cases, the difference in final deflection distance must therefore be a result of the droplet dynamics that occur after the droplet passes the transition. Following the 30° to 3° transition,

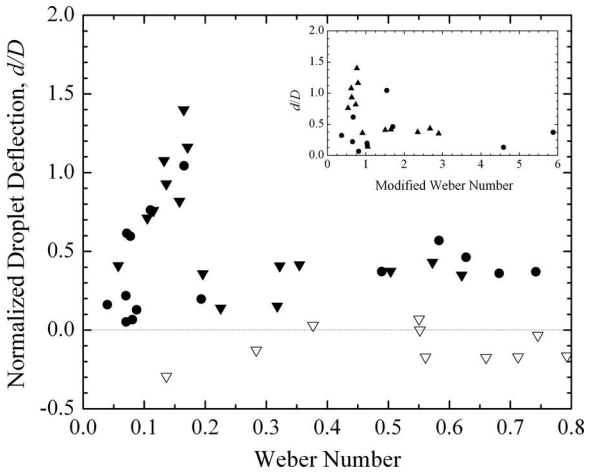

FIG. 6. Normalized droplet deflection as a function of Weber number for single contact angle hysteresis transitions from (▼) 30° to 3°, (●) 15° to 3°, and from (▽) 3° to 30° all at a transition angle of $\alpha_T = 40°$. The inset contains the same data plotted against the modified Weber number proposed in Eq. (5).

the droplet passes onto a surface with much less drag than the following 3° to 30° transition. As seen in Figure 2 the drag on the 3° surface is roughly one-third the drag on the 30° contact angle hysteresis surface. The force resulting from the receding contact line motion is imposed only as the drop passes the transition while the gravitational driving force is constant. As a result, the lateral motion induced by the transition decays away more quickly on the surface with higher contact angle hysteresis and larger drag coefficients resulting in a reduced overall droplet deflection even though the initial deflection angles are identical in both cases.

The difference in deflection can be calculated from first principles. Assuming a constant deceleration, a_y, on the sanded Teflon surfaces, the deflection, $d = 1/2\ a_y t_f^2 + V_i t_f$, can be shown to be dependent on the initial lateral velocity imposed on the drop by the transition, V_i, and the time for the drop to lose all its lateral velocity, $t_f = -V_i/a_y$. The deceleration can be taken from the measurements in Figure 2, $a_y = g_x - a_{drop}$, or from the predictions of theory in Eq. (2). The initial velocity can be calculated from a simple energy argument assuming that the deflection force is exerted over a finite distance which we estimate as the radius of the contact between the drop and the surface, $R \sin(\pi - \theta)$. If we assume complete conversion of work performed at the transition into kinetic energy of the drop, the initial lateral velocity becomes

$$V_i \approx \sqrt{\frac{3\gamma\ (\cos(\theta_R)_1 - \cos(\theta_R)_2)\ \sin^2(\pi - \theta)\ \sin(\alpha_T)}{2\pi\rho R}}. \tag{4}$$

Using Eq. (4) to calculate the deflection of a drop across a $\alpha_T = 40°$ transition, one finds a maximum possible deflection of about $d/D \approx 1.4$ for a 30° to 3° hysteresis transition, $d/D \approx 0.7$ for a 15° to 3° hysteresis transition, and about $d/D \approx -0.20$ for a 3° to 30° hysteresis transition independent of Weber number. These calculations predict the extreme values of deflection in Figures 5 and 6 reasonably well but do not represent all the data because this calculation ignores the dynamics and assumes that all of the energy is transferred between interfacial and kinetic energy of the drop.

A number of other observations can be made from the data in Figure 5. Increasing the difference in the contact angle hysteresis across the transition was found to increase the deflection. However, when a droplet transitions onto a surface with a contact angle hysteresis of $\theta_H = 50°$, which is large enough to completely halt droplet motion, the droplet deflection is clearly minimized independently of transition angle. At small Weber numbers, the droplet is captured just beyond the transition line. We can also observe that, for the transitions investigated, a maximum in deflection is observed at a transition angle of approximately $\alpha_T \approx 40°$. The maximum deflections were observed for droplets starting on a surface with 30° contact angle hysteresis and then transitioning to a surface of 3° contact angle hysteresis. For these surfaces of a transition angle of $\alpha_T = 40°$, a significant

deflection was achieved over a wide range of Weber numbers, with a maximum observed deflection of $d/D = 1.4$. This deflection is sufficient to achieve efficient sorting, as it exceeds what we consider the minimum deflection of one diameter required to effectively sort drops. However, effective sorting also requires the chosen device to be selective. For that reason, the Weber number dependence of the droplet deflection was also investigated.

In Figure 6, the normalized droplet deflection is shown as a function of Weber number for a transition angle of $\alpha_T = 40^\circ$ for transitions from 30° to 3° contact angle hysteresis, 3° to 30° contact angle hysteresis, and 15° to 3° contact angle hysteresis. For the 30° to 3° and the 15° to 3° contact angle hysteresis transitions, a clear maximum is observed in the deflection data with Weber number at 0.15. The droplets are found to reach a maximum deflection of $d/D = 1.4$ and $d/D = 1.1$ for 30° to 3° and 15° to 3°, respectively. Additionally, only within a very narrow range of Weber numbers, $0.1 < We < 0.2$, was the deflection found to be large enough to deflect the droplet by more than a single diameter to either side. Outside of this range, the deflection is much less substantial, $d/D < 0.5$, and is essentially independent of the Weber number. Finally, note that no deflection data are presented for $We < 0.05$ because at these low velocities it was difficult to mobilize the droplets on the surface with 30° contact angle hysteresis. At larger Weber numbers, the inertial forces are much larger than the deflection force imparted on the drop as it crosses the transition. This can be better seen if a new modified Weber number is formulated which directly compares the inertial force to the difference in sticking force experienced by the drop as it crosses the transition as defined in Eq. (5),

$$We_{\text{mod}} = \frac{\rho U^2 D}{\gamma[\cos(\theta_R)_1 - \cos(\theta_R)_2]\sin(\alpha_T)}. \tag{5}$$

For the new modified Weber number, the optimal range for large deflections occurs for $0.75 < We_{\text{mod}} < 1.0$ as seen in the inset of Figure 6.

The presence of this maximum deflection explains the spread in the data in Figure 5, which incorporated data over a wide range of Weber numbers including the optimal values. No maximum was observed for the transitions from low contact angle hysteresis to higher contact angle hysteresis over the range of Weber numbers accessible in these experiments. In fact, over for transitions from 3° to 30° hysteresis the value of deflection is constant at roughly the value of $d/D \approx -0.13$ predicted by our theoretical analysis. This is likely because as the drop transitions from low to high hysteresis, the interfacial energy of the drop can only be increased by reducing the velocity of the drop and changing its kinetic energy. As a result, the assumption of perfect conversion of kinetic energy to interfacial energy is reasonable. However, when the droplet transitions from high hysteresis to low hysteresis, the assumption of perfect conversion of interfacial energy into kinetic energy of the drop clearly does not hold over all Weber numbers. This is because the interfacial energy can transfer not only to kinetic energy of the drop but also to capillary waves on the surface of the drop or to the mixing and swirling of fluid within the drop. As a result, the efficiency of energy conversion is not perfect but is extremely sensitive to the droplet dynamics as it crosses the transition. One might expect the efficiency of energy transfer would be maximized if dynamics of transition excited the droplet at its natural frequency. In other words, at $We \simeq 0.15$, the non-dimensional natural frequency should be approximately one, $f_n t_c = f_n R \sin(\pi - \theta_1)/U \approx 1$, where t_c is the residence time for the drop crossing the transition in contact angle hysteresis. This is in fact the case. For the transitions from 30° to 3° hysteresis transition at the peak Weber number of $We = 0.17$, the drop takes approximately $t_c = 0.023$ s ($1/t_c = 44$ Hz) to cross the transition. The resonance frequency of a water drop has been measured on the 3° hysteresis surfaces to be $f_n = 55$ Hz.[10] For the 15° to 3° transition, the results are even closer with $1/t_c = 50$ Hz at $We = 0.17$. Thus, it appears the maximum deflection is achieved when the transition excites the droplet at or near its resonance frequency.

A number of additional experiments were performed examining transitions at $We \simeq 0.15$ for a range of transition angles with droplets transitioning from 30° to 3° contact angle hysteresis. The maximum droplet deflections were found to increase with increasing transition angle as predicted by our theoretical analysis in Eq. (3). However, experiments for which the transition angles were much greater than 45°, were experimentally challenging to perform consistently. The droplet deflections

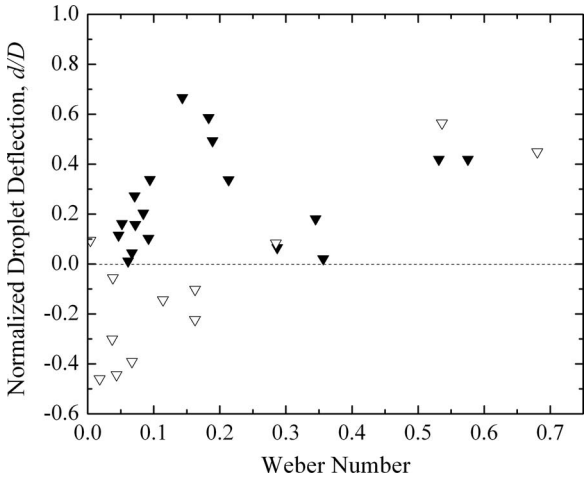

FIG. 7. Deflection of drops moving over a stripe of varying contact angle hysteresis presented as a function of the Weber number at a transition angle of $\alpha_T = 40^\circ$. The data include (▼) a 3.5 mm stripe of 3° hysteresis among a surface with 30° hysteresis and (∇) a 3.5 mm stripe of 30° hysteresis among a surface of 3° hysteresis.

measured at these angles were not universally reproducible and the resulting data had large standard deviations.

A natural extension of this work is to ask what occurs when a drop moves across a stripe or multiple stripes of different contact angle hysteresis, instead of a single transition. The addition of a stripe means that a droplet will undergo two transitions in the course of travel, one from low to high and another from high to low contact angle hysteresis. Of the surfaces tested, the maximum deflection of any water droplet was observed on surfaces of 3° and 30° contact angle hysteresis, so only stripes varying between those surfaces were considered so that the observed deflection could be maximized. The stripe widths were on the order of the droplet diameter, $w = 3.5$ mm, allowing for full wetting on the stripe as the droplet passed over it. The maximum observed droplet deflections were observed to occur at a transition angle of 40°. This is in agreement with the results for the single transition.

In Figure 7, the deflection of droplets moving past single stripes of 3° contact angle hysteresis on a background of 30° contact angle hysteresis and vice versa are presented for a transition angle of $\alpha_T = 40^\circ$ for a range of Weber numbers. Here, the Weber number and transition angle are always evaluated using the velocity of the drop as it encounters the first transition. As described previously, a single transition from higher to lower contact angle hysteresis produces a deflection to the left and a single transition from lower to higher contact angle results in a deflection to the right. For the case of a stripe, the net droplet deflection is sum of the deflections produced by both transitions. As seen in Figure 7, the deflection is consistently to the left for the case of a stripe with 3° contact angle hysteresis on a surface of 30° hysteresis. The first transition the drop experiences from 30° to 3° hysteresis produces a deflection that is to the left, and as seen in Figure 5, always larger in magnitude than the right deflection of the 3° to 30° hysteresis transition at a given Weber number. Following the first transition, the droplet encounters the second transition with increased Weber number and at a smaller transition angle, $\alpha_T < 40^\circ$, resulting in a small secondary deflection back to the right. As was observed for a single transition, a maximum deflection is observed for $We \simeq 0.15$, although due to the presence of the second transition, a maximum deflection of only $d/D \sim 0.8$ was observed.

The trends in the deflection data of droplets passing over a stripe of 30° contact angle hysteresis on a surface of 3° hysteresis are more complex. At smaller Weber numbers, $We < 0.2$, the net droplet deflection is to the right. The initial transition from 3° to 30° hysteresis causes a deflection to the right. Due to the absorption of kinetic energy at the first transition, the droplet slows between the first and second transition. The droplet thus moves along the stripe and encounters the second transition at a lower angle and Weber number. At low Weber numbers, the deflection at the second hysteresis transition is minimal and a net deflection to the right is observed. However, for larger

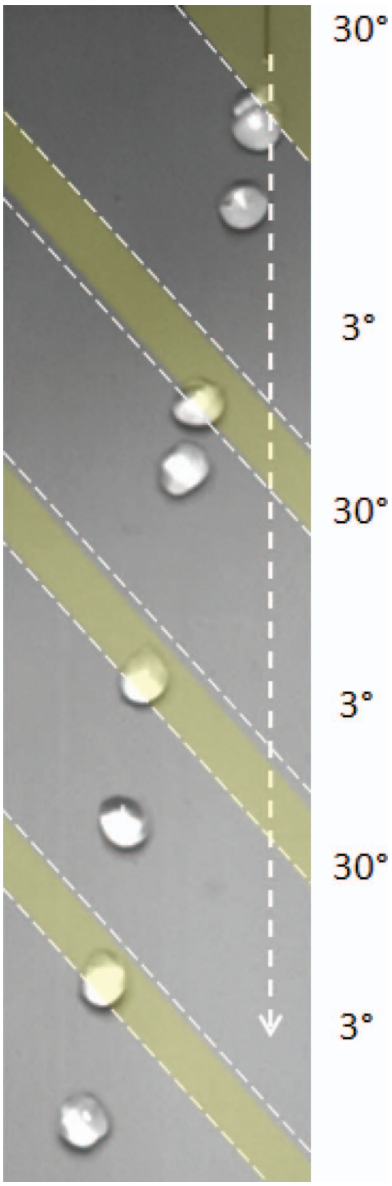

FIG. 8. A low contact angle hysteresis surface with high hysteresis stripes of 3.5 mm in width. The resulting deflection is many times that of a single transition. The Weber number at the first stripe is $We = 0.15$, which is near the range of maximum deflection. Subsequent stripes result in further droplet deflection, however, each contribution is diminished because the droplet encounters them at higher Weber numbers.

Weber numbers, the first transition still creates a small deflection, but the deceleration of the drop is enough to reduce the Weber number to within the optimal range at the second transition. The result is a smooth variation from right or negative drop deflections at low Weber number to left or positive deflections as the Weber number increases beyond $We > 0.25$.

If a single stripe can produce measureable droplet deflections near the ideal Weber number and transition angle, then it follows that a series of stripes can be used in series to further amplify the response of the drop. In Figure 8, a device designed to maximize droplet deflection by incorporating multiple stripes on a surface is presented. This device achieves far more deflection than a single transition or a single stripe, by having parallel stripes of 30° hysteresis across a surface of 3° hysteresis. The result is a droplet deflection of $d/D = 3.5$ after 60 mm of travel past 3 stripes. The droplet moves across the first transition at a Weber number of 0.15. This leads to the maximum

possible initial deflection. However, as the drop continues to accelerate down the device, the Weber number at each subsequent stripe increases and the deflection from each of the subsequent stripes is smaller. Even so, as it is clearly shown in Figure 9, multiple stripes of different receding contact angles can be a very effective means of deflecting or even sorting drops on a two-dimensional digital microfluidics platform.

IV. CONCLUSION

In this paper, the ability for sharp transitions in contact angle hysteresis to deflect droplets was investigated. It was shown that for a single transition, droplet deflection of more than one droplet diameter were possible. Superhydrophobic sanded Teflon was shown to be an excellent platform for these two-dimensional digital microfluidics experiments because of its high advancing contact angles and the ease in which variations in contact angle hysteresis could be achieved. By masking patterns onto the Teflon, sharp transitions in contact angle hysteresis were created using different grit-designation sand paper to create variations in surface roughness. We show that a drop moving over these sharp transitions in contact angle hysteresis experiences a small force from the contact line transition. This force results from the conversion of kinetic energy to interfacial energy and vice versa as the change in contact angle hysteresis transforms the shape of the drop. Orienting the transition at an angle to the principle direction of the drop results in a force normal to the transition line, deflecting the droplet from its original path. The sign of the force and thus the direction of this deflection are shown to depend on whether the drop transitions onto a surface of a higher or lower receding contact angle. The drop deflects towards the transition line when moving from a higher to lower receding contact angle surface, while when transitioning from a lower to a higher receding contact angle surface the drop deflects away from the transition line. The initial angle of deflection is identical in both cases. However, higher hysteresis on the downstream surface mutes the impact of the deflection force because it has higher surface drag, resulting in decreased overall deflection. It is shown that this deflection is a function of the magnitude of contact angle hysteresis difference, the angle of the transition, and the Weber number of the drop. In this study, the optimal conditions for deflecting water droplets sliding on sanded Teflon were found using a transition from a surface region with 30° contact angle hysteresis to 3° at Weber number around $We \approx 0.15$. In our study, a transition angle of around 40°, but theory predicts that the deflection should increase with further increases in transition angle. Small changes in Weber number can have a significant effect on the deflection, with Weber numbers outside of $0.1 < We < 0.2$ experiencing minimal deflection when transitioning from 30° to 3° or 15° to 3° contact angle hysteresis. Within this range of Weber numbers the transition time was found to coincide with one over the resonance time of the drop. As a result, at these speeds the interfacial energy released by the receding contact line is most efficiently transferred into kinetic energy of the drop thereby maximizing its deflection.

It is possible to achieve measureable deflections with the addition of a stripe of different contact angle hysteresis alternating between 3° and 30°. The effect of encountering each transition is found to be additive. Finally, it is shown that a series of stripes can achieve even larger droplet deflections. This work has thus clearly shown that with both single contact angle hysteresis transitions and stripes of differing contact angle hysteresis, it is possible to target drops of particular size, velocity, and wettability and alter their path sufficiently to effectively sort droplets. In combination with our previous work in this area, we have now shown that superhydrophobic Teflon surfaces are an excellent platform for two-dimensional digital microfluidics, as it has now been shown to successfully perform many of the tasks needed for effective development of these microfluidic devices. This includes droplet coalescence and mixing,[10] and the motion, deflection, and sorting of droplets shown here.

[1] G. M. Whitesides, "The origins and the future of microfluidics," Nature (London) **442**, 368 (2006).
[2] D. R. Reyes, D. Iossifidis, P. A. Auroux, and A. Manz, "Micrototal analysis systems. 1. Introduction, theory, and technology," Anal. Chem. **74**, 2623 (2002).
[3] H. A. Stone and S. Kim, "Microfluidics: Basic issues, applications, and challenges," AIChE J. **47**, 1250 (2001).
[4] H. A. Stone, A. D. Stroock, and A. Ajdari, "Engineering flows in small devices: Microfluidics toward a lab-on-a-chip," Annu. Rev. Fluid Mech. **36**, 381 (2004).

[5] T. M. Squires and S. R. Quake, "Microfluidics: Fluid physics at the nanoliter scale," Rev. Mod. Phys. **77**, 977 (2005).
[6] A. Manz, D. J. Harrison, E. M. J. Verpoorte, J. C. Fettinger, A. Paulus, H. Ludi, and H. M. Widmer, "Planar chips technology for miniaturization and integration of separation techniques into monitoring systems: Capillary electrophoresis on a chip," J. Chromatogr. **593**, 253 (1992).
[7] X. Zhang, F. Shi, J. Niu, Y. G. Jiang, and Z. Q. Wang, "Superhydrophobic surfaces: From structural control to functional application," J. Mater. Chem. **18**, 621 (2008).
[8] M. A. Nilsson, R. J. Daniello, and J. P. Rothstein, "A novel and inexpensive technique for creating superhydrophobic surfaces using Teflon and sandpaper," J. Phys. D **43**, 045301 (2010).
[9] J. P. Rothstein, "Slip on superhydrophobic surfaces," Annu. Rev. Fluid Mech. **42**, 89 (2010).
[10] M. A. Nilsson and J. P. Rothstein, "The effect of contact angle hysteresis on droplet coalescence and mixing," J. Colloid Interface Sci. **363**(2), 646 (2011).
[11] C. Neinhuis and W. Barthlott, "Characterization and distribution of water-repellent, self-cleaning plant surfaces," Ann. Bot. (London) **79**, 667 (1997).
[12] J. Bico, C. Marzolin, and D. Quere, "Pearl drops," Europhys. Lett. **47**, 220 (1999).
[13] W. Chen, A. Y. Fadeev, M. C. Hsieh, D. Oner, J. Youngblood, and T. J. McCarthy, "Ultrahydrophobic and ultralyophobic surfaces: Some comments and examples," Langmuir **15**, 3395 (1999).
[14] J. W. Kim and C. J. Kim, "Nanostructured surfaces for dramatic reduction of flow resistance in droplet-based microfluidics," IEEE Proc. **2002**, 479.
[15] M. Sakai, J. H. Song, N. Yoshida, S. Suzuki, Y. Kameshima, and A. Nakajima, "Direct observation of internal fluidity in a water droplet during sliding on hydrophobic surfaces," Langmuir **22**, 4906 (2006).
[16] A. Shastry, M. J. Case, and K. F. Bohringer, "Directing droplets using microstructured surfaces," Langmuir **22**, 6161 (2006).
[17] D. Richard and D. Quere, "Viscous drops rolling on a tilted non-wettable solid," Europhys. Lett. **48**, 286 (1999).
[18] L. Mahadevan and Y. Pomeau, "Rolling droplets," Phys. Fluids **11**, 2449 (1999).
[19] S. Gogte, P. Vorobieff, R. Truesdell, A. Mammoli, F. van Swol, P. Shah, and C. J. Brinker, "Effective slip on textured superhydrophobic surfaces," Phys. Fluids **17**, 051701 (2005).
[20] M. Reyssat, D. Richard, C. Clanet, and D. Quere, "Dynamical superhydrophobicity," Faraday Discuss. **146**, 19 (2010).
[21] M. K. Chaudhury and G. M. Whitesides, "How to make water run uphill," Science **256**, 1539 (1992).
[22] Y. Ito, M. Heydari, A. Hashimoto, T. Konno, A. Hirasawa, S. Hori, K. Kurita, and A. Nakajima, "The movement of a water droplet on a gradient surface prepared by photodegradation," Langmuir **23**, 1845 (2007).
[23] C. Sun, X. W. Zhao, Y. H. Han, and Z. Z. Gu, "Control of water droplet motion by alteration of roughness gradient on silicon wafer by laser surface treatment," Thin Solid Films **516**, 4059 (2008).
[24] K. A. Wier, L. C. Gao, and T. J. McCarthy, "Two-dimensional fluidics based on differential lyophobicity and gravity," Langmuir **22**, 4914 (2006).
[25] M. G. Pollack, R. B. Fair, and A. D. Shenderov, "Electrowetting-based actuation of liquid droplets for microfluidic applications," Appl. Phys. Lett. **77**, 1725 (2000).
[26] T. N. Krupenkin, J. A. Taylor, T. M. Schneider, and S. Yang, "From rolling ball to complete wetting: The dynamic tuning of liquids on nanostructured surfaces," Langmuir **20**, 3824 (2004).
[27] D. R. Link, E. Grasland-Mongrain, A. Duri, F. Sarrazin, Z. D. Cheng, G. Cristobal, M. Marquez, and D. A. Weitz, "Electric control of droplets in microfluidic devices," Angew. Chem., Int. Ed. **45**, 2556 (2006).
[28] Y. Li, Y. Q. Fu, B. W. Flynn, W. Parkes, Y. Liu, S. Brodie, J. G. Terry, L. I. Haworth, A. S. Bunting, J. T. M. Stevenson, S. Smith, and A. J. Walton, "Test Structures for characterising the integration of EWOD and SAW technologies for microfluidics," IEEE Proc. **2010**, 52.
[29] S. Suzuki, A. Nakajima, K. Tanaka, M. Sakai, A. Hashimoto, N. Yoshida, Y. Kameshima, and K. Okada, "Sliding behavior of water droplets on line-patterned hydrophobic surfaces," Appl. Surf. Sci. **254**, 1797 (2008).
[30] A. D. Stroock, S. K. Dertinger, A. Ajdari, I. Mezic, H. A. Stone, and G. M. Whitesides, "Chaotic mixer for microchannels," Science **295**, 647 (2002).
[31] A. D. Stroock, S. K. Dertinger, G. M. Whitesides, and A. Ajdari, "Patterning flows using grooved surfaces," Anal. Chem. **74**, 5306 (2002).
[32] J. Ou, G. R. Moss, and J. P. Rothstein, "Enhanced mixing in laminar flows using ultrahydrophobic surfaces," Phys. Rev. E **76**, 016304 (2007).
[33] A. B. D. Cassie and S. Baxter, "Wettability of porous surfaces," Trans. Faraday Soc. **40**, 0546 (1944).
[34] R. N. Wenzel, "Resistance of solid surfaces to wetting by water," Ind. Eng. Chem. **28**, 988 (1936).